Direct Yellow 8 Azo Removal by Bentonite Clay Solution: Experimental and Theoretical Studies

Sanaa Tareq[1], Masar Ali Awad[2], Khawla Kani Jasim[3], Shahad Kadhim Taher[4], Mustafa M. Kadhim[5*]

Abstract

In the theoretical part, removal of direct yellow 8 (DY8) from water solution was accomplished using Bentonite Clay as an adsorbent. Under batch adsorption, the adsorption was observed as a function of contact time, adsorbent dosage, pH, and temperature. The equilibrium data were fitted with the Langmuir and Freundlich adsorption models, and the linear regression coefficient R2 was used to determine the best fitting isotherm model. thermodynamic parameters of the ongoing adsorption mechanism, such as Gibb's free energy, enthalpy, and entropy, have also been measured. The batch method was also used for the kinetic calculations, and the day's adsorption assumes first-order rate kinetics. The kinetic studies also show that the intraparticle diffusion process was active. Density Functional Theory (DFT) was used to study the dye structure with Gaussian 09 and predict the active site in a molecule using total electron density (TED) and electrostatic surface potential (ESP).

Key Words: Adsorption, Direct Yellow 8, Bentonite, DFT, TED.

DOI Number: 10.14704/nq.2021.19.5.NQ21056 **NeuroQuantology 2021; 19(5):120-131**

Introduction

Concerns have been raised over synthetic effluents containing organic dyes and toxic compounds contaminating water supplies [Onélia A et al, 2013; Kareem et. Al 2016]. Environmental pollution has been identified as one of the most serious problems confronting contemporary society, owing primarily to population growth and increased industrial activity (Colpini L.M.S et al, 2008-Zhang F. et al, 1998). Dyeing, paper and pulp, textiles, plastics, leather, cosmetics, and food industries have all long used dyes. These factories' effluents face some risks and environmental issues. This industries' wastewater could pose an exotoxin threat and introduce the possibility of bioaccumulation, which may potentially affect humans. Also trace quantities of dyes, up to many parts per million (ppm), are unacceptable because they alter the color of the water and render it unusable for domestic and technical purposes. Numerous dyes are non-biodegradable, which reduces sunlight from reaching into the water and thereby inhibits photosynthesis. Furthermore, since such dyes are mutagenic and carcinogenic to living organisms, their inclusion in water may have a detrimental effect on them (Derudi, M et al, 2007). Due to the wide range of dyes used in manufacturing, there is no universal method for removing them from wastewater. The most successful technologies incorporate physical, chemical, and biological processes, and their selection is dependent on a variety of factors (such as the form and concentration of the dye, the chemical structure of the sewage, the presence of additional impurities, or the process's cost) (Erdem, B et al, 2016). Adsorption is now the most widely used method due to its simplicity of operation, low cost, and high performance (Enaas Abdul Hussein et al, 2020).

Corresponding author: Mustafa M. Kadhim

Address: [1]Department of Chemistry, College of Science for Women, University of Baghdad, Baghdad, Iraq; [2]Department of Chemistry, College of Science, Al_Muthanna University, Al_Muthanna, Iraq; [3]Department of Chemistry, College of Science, Al_Muthanna University, Al_Muthanna, Iraq; [4]Department of Chemistry, College of Science for Women, University of Baghdad, Baghdad, Iraq; [5*]Department of Dentistry, Kut College University, Kut, Wasit, Iraq.

[5*]E-mail: mustafa_Kut88@yahoo.com, mustafa.mohammed@alkutcollege.edu.iq

Relevant conflicts of interest/financial disclosures: The authors declare that the research was conducted in the absence of any commercial or financial relationships that could be construed as a potential conflict of interest.

Received: 14 March 2021 **Accepted:** 15 April 2021

Density functional theory (DFT) [Von U et al, 2013] has developed an extremely valuable paradigm for creating novel guidelines for rationalizing, modeling, and ultimately comprehending a wide variety of chemical processes (Gece G et al, 2015). Numerous chemical terms that are now commonly used as descriptors of chemical reactivity, for example, electronegativity hardness or softness numbers, occur spontaneously within DFT. The effects of solvent ions, the surface structure, and adsorption of metal atoms, or sites or vacancies for oxides, active liquid-phase adsorption, and solubility are only a few of the parameters that have been overlooked (Udhayakala P et al, 2013; Ennas Abdul Hussein et al, 2020).

Materials and Methods

Fluk, BDH, and Sigma Aldrich supplied the chemicals used. Shimadzu spectrophotometer. UV-1800PC Shimadzu recorded UV-Visible spectra

The Adsorbate

Direct yellow 8, CAS 10130-29-7, Empirical Formula C24H19N4NaO5S2, and Molecular Weight 530.55 **Figure 1** illustrates the chemical composition of direct yellow 8.

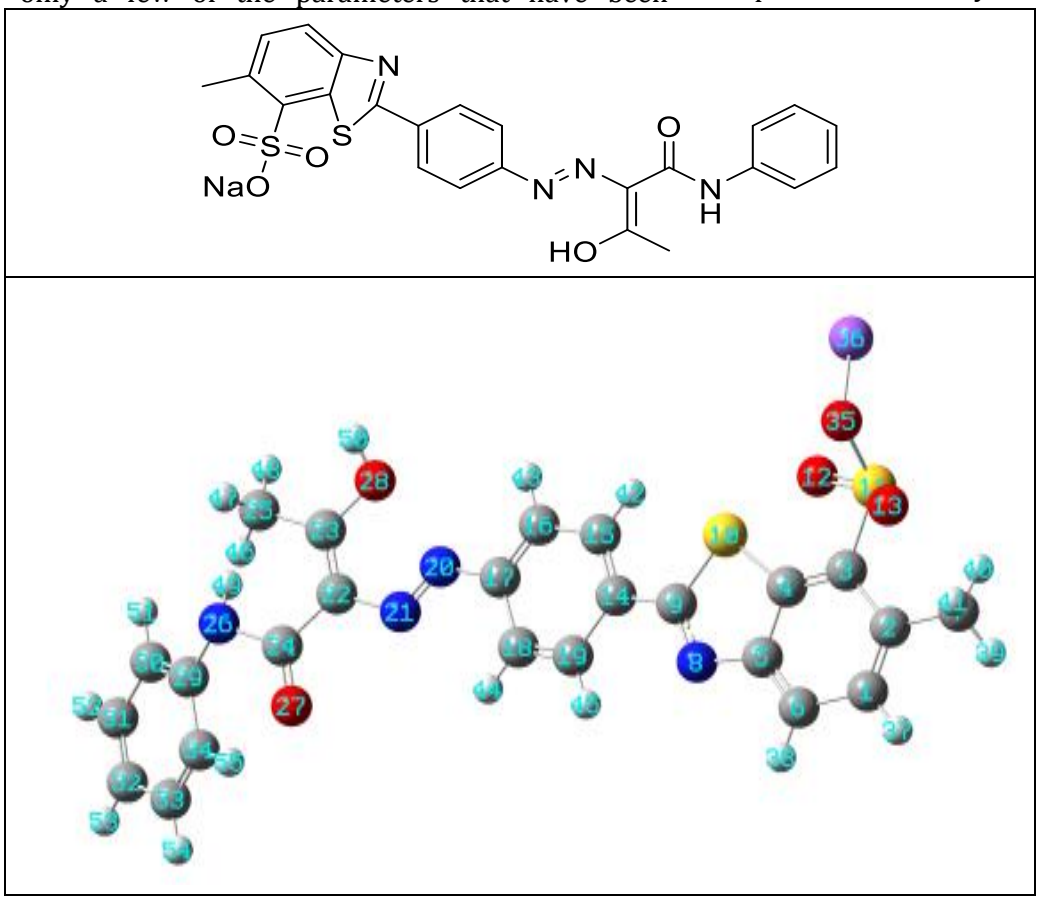

Figure 1. The chemical structure of direct yellow 8.

The Adsorbent

Bentonite clay was used as an adsorbent in this analysis and was collected from the General Company for Geological Survey and Mining, Ministry of Industry and Minerals, Baghdad, Iraq. The clay rock was ground and sieved to produce particles with a particle size of (106-212) micrometer. The sieved samples were washed with purified water and then dried at a temperature of 20 degrees Celsius for 24 hours. Both tests and analysis were conducted using this clay.

Spectrophotometric Determination

The adsorbate was analyzed spectrophotometrically by the appropriate method to determine the wavelength at maximum absorption (λ_{max}), absorption spectrum for dye by using UV-visible spectrophotometer has been recorded in the range (200-1100 nm) by using quartz cell (Cuvette) of 1cm thickness (path length. The spectra of DY8 are shown in **Figure 2**.

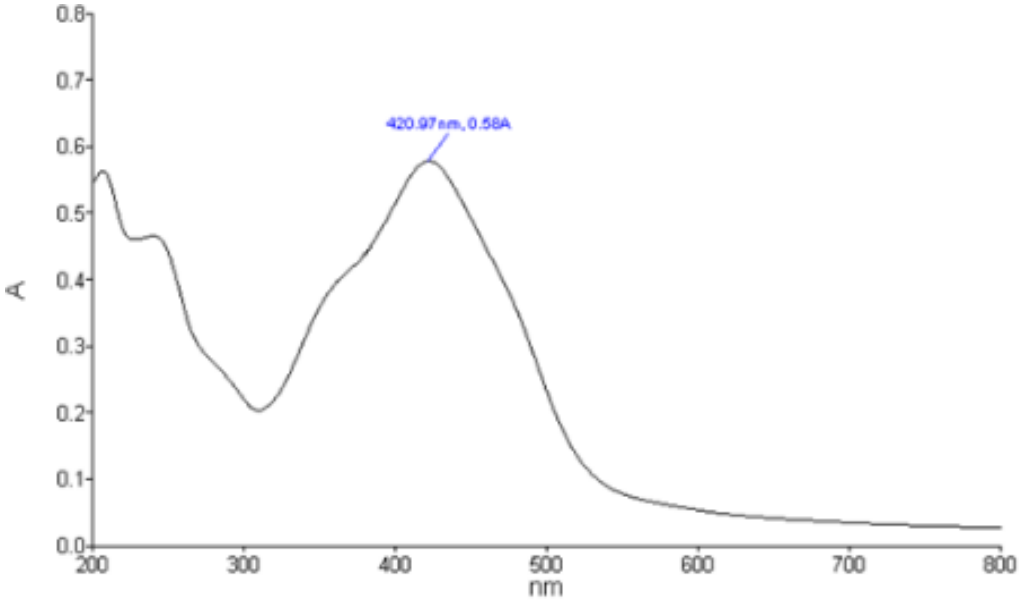

Figure 2. The scan spectrum curve of DY

The calibration curve was determined by fixing the λ_{max} that obeys the (Lambert beer's law) at specific concentrations prepared for dye. After that, the absorption has been recorded and a calibration curve plotted between absorption and concentration, the best line between points has been drawn using the least square method. Figure 3 shows the calibration curves for DY8.

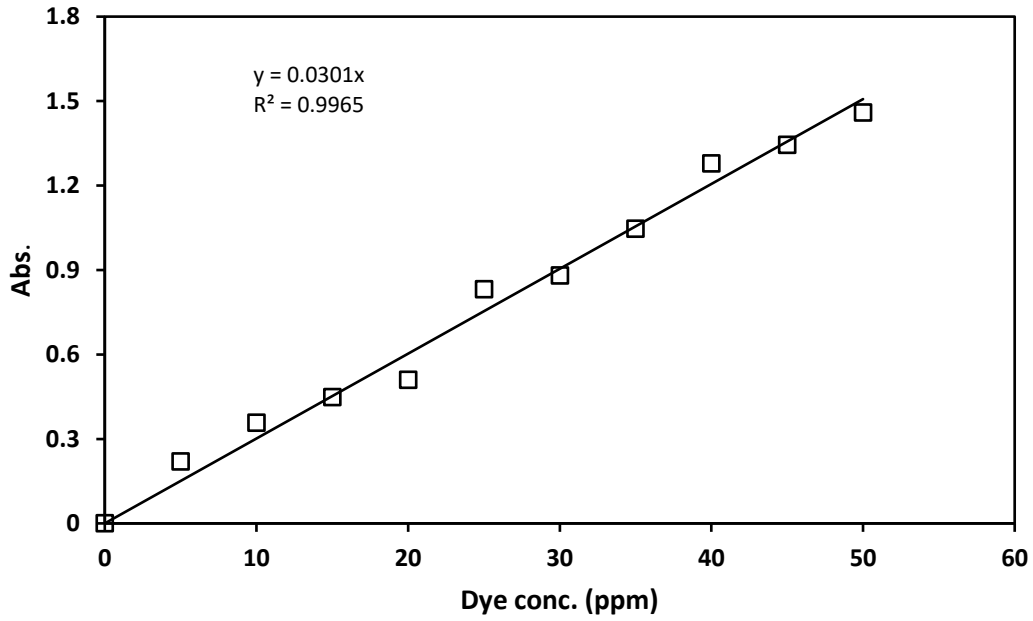

Figure 3. The calibration curve of CIP

Preparation of Stock Solution

The concentration of a stock aqueous solution of direct yellow (100 ppm) was established by dissolving (100 g) of direct dye in (250 ml) bustle ethanol, and the dye's maximal absorbance wavelength was determined using the UV-Visible spectrophotometer to be between 250 and 700 nm. The standard curve for the dye of choice was prepared at concentrations ranging from 5 to 50 ppm and used to determine the dye concentration in ethanoic solution.

Adsorption Isotherms

To evaluate the dye's adsorption isotherm, (5), conical flasks have been used, containing (0.2 gm) of adsorbent. Then (100) mL of adsorbate solution has been added into each of the flasks, which have a concentration ranged between (5 -50) (mg/L) for

dye. After closing, the flasks were shaken with a water bath shaker at a constant temperature according to the equilibrium time of the adsorption. Then, they are centrifuged for 15 minutes, UV-Vis spectrophotometer has been used to measure the absorbance for the solutions at the convenient wavelength for dye. The values obtained of absorbance have been used to determine the equilibrium concentration from the calibration curve. The adsorbate quantities were calculated in all experiments according to equation (1) [Ennas Abdul Hussein et al, 2020].

$$q_e = \frac{(C_0 - C_e)\, v}{w} \qquad (1)$$

Where qe denotes the quantity of drug adsorbed per unit weight of adsorbent (mg/g); C0 denotes theoriginal dye concentration (mg/L); Ce denotes the dye concentration in solution at equilibrium time (mg/L); (V) denotes the solution volume L, and m denotes the adsorbent dose (g).

Investigate the Impact of pH on the Direct Adsorption of Compounds

Adsorption tests at various pH values were conducted to establish the influence of pH on the adsorption of dye solution (4, 6, and 10). The pH of the media was preserved between acidic and alkaline by applying the appropriate quantities of dilute (0.1M) hydrochloric acid and sodium hydroxide solutions. While conducting the tests, the dye concentration, adsorbent dose, and equilibrium duration were held steady. A pH meter was used to determine the pH of the samples.

Effect of Amount of Adsorbate

Initial dye concentration of (ppm) for DY was used in conjunction with adsorbent dose 0.2, 0.4, 0.6, 0.8, and 1 gm. Contact time, pH, temperature, and particle size of 30 minutes, (298) K, and from 106 to 212 micrometer respectively were kept constant according to equation (2-8).

Determination of Equilibrium Time

A 0.2 gm of clay was added to a 250 ml conical flask. After adding (100) ml of adsorbate solution containing (20) ppm DY, the flask was fixed in a water route shaker at a constant temperature. The initial time was then counted, and every ten minutes afterward, a sample was pipit and put in the centrifuge for fifteen minutes (at 3000 rpm). A supernatant has been separated by decantation and the absorption of the solution has been recorded at λmax sample. The process has been achieved repeatedly to the equilibrium. The contact time and temperature were kept constant according to equation (1) [Enaas ABD-Al-Hussien et al, 2012].

Study the Temperature effect on the Bis-azo compound Adsorption

Adsorption equilibrium experiments were performed to determine the influence of temperature on dye adsorption on clay using 0.2 g of adsorbent and 100 ml of varying dye concentrations in equal conical flasks at five different temperatures (25, 35, 45, and 55) °C. After adding the dye solution to the flint clay, the reaction mixtures were stirred for 30 minutes at 200 rpm in a water bath shaker. After 90 minutes, 10 mL of each flask was sampled, centrifuged for 15 minutes at 3000 rpm, and the dye concentration was determined using a UV–visible spectrophotometer.

Calculations Models

The measurements were performed in vacuum using the Gaussian 09 software (Weigend F et al, 2005) and DFT with the B3LYP hybrid functional (Ennas Abdul Hussein et al, 2020- Lee C et al, 1988). For both atoms, the triple-z basis set 6-311G (d,p) is used. Additionally, the electrostatic potential (ESP) charges are measured to obtain maps of the molecular electrostatic potential (MEP). These maps were used to calculate the electron delocalization on the molecular surface [McIver W et al, 2005].

Results and Discussion

Adsorption of Congo Red Effect of Variable Parameters:

Equilibrium Time

We investigated the impact of contact time on the volume of DY8 adsorbed per unit of adsorbent at a constant temperature, pH, and concentration. The equilibrium period for DY8 20(ppm) at 25 °C and pH=4 is shown in Figure 4.

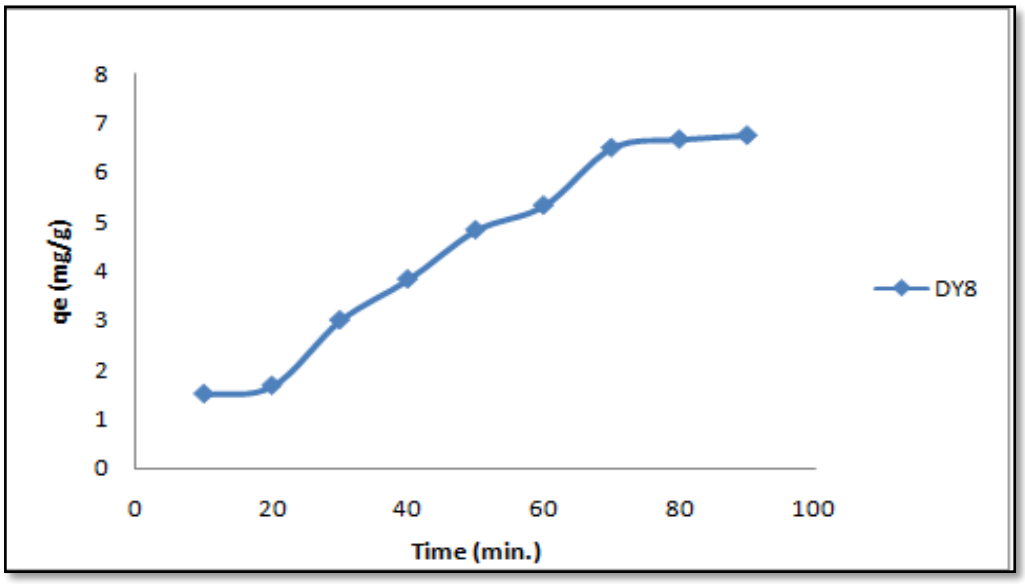

Figure 4. The effect of contact time on the adsorption of DY8 at 25 C

At 10 minutes, a sudden rise in adsorption is observed, followed by a steady increase in adsorption with rising contact duration up to 90 minutes, at which point a maximum value of adsorption is achieved. Following this period, the amount of dye adsorbed was negligible: very slight decreases for dye adsorbed were detected, suggesting desorption. As a result, the optimal contact time is set at 90 minutes. Similar findings have been published for DY8 adsorption on calcium-rich clay ash and malachite green dye adsorption on acid-activated low-cost carbon. (Abida Kausar et al, 2018).

Dose of Adsorbent

The impact of adsorbent weight on Congo red dye adsorption was investigated by varying the volume of adsorbent (0.2, 0.4, 0.6, 0.8, and 1g, per 100 mL) in the test solution while maintaining a constant initial dye concentration (25 ppm) and contact duration (90 minutes). Figure 5 illustrates the results.

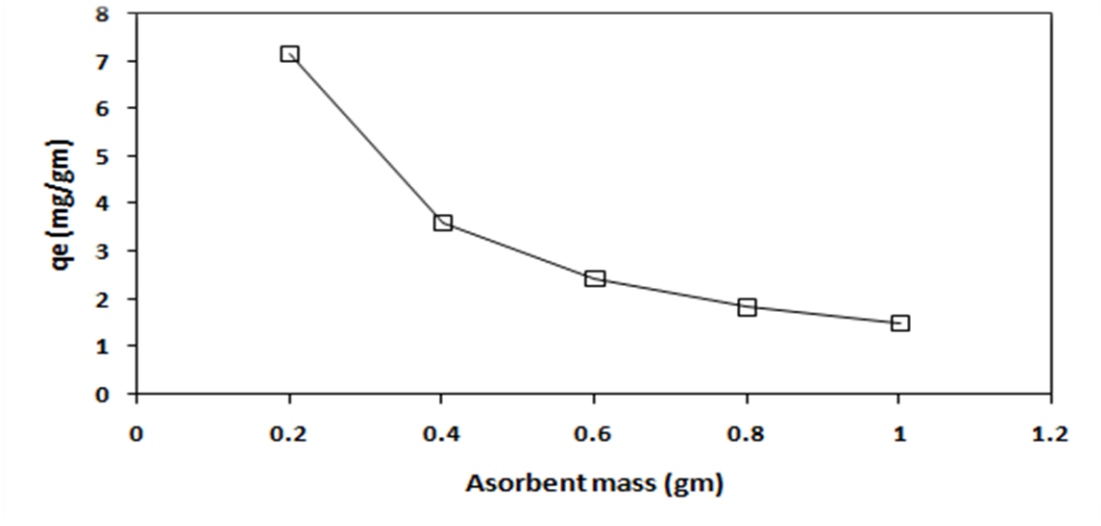

Figure 5. Effect of adsorbent dosage on removal of DY dye.

It is obvious that the percentage elimination of the dye (qi) reduces as the adsorbent dosage increases, but above a value of 0.2 g, qe approaches a maximal value. This is more likely attributed to an improved supply of exchangeable sites or an increased surface region for adsorption [Aderonke Ajibola et al,]. As shown in Figure 5, the optimal clay dose for DY removal is 0.2 gm per 100mL. As a result, both tests were conducted with 0.2 gm of adsorbent.

Effect of pH

At pH 4, 6, and 10, adsorption tests were conducted. The pH of the media was preserved between acidic and alkaline by applying the appropriate concentrations of dilute hydrochloric acid and sodium hydroxide solutions. The dye concentration (5-25) ppm, adsorbent dose, and temperature (25)°C were both held stable during the experiments. Figures 6 and 7 illustrate the role of pH on the removal of DY dye.

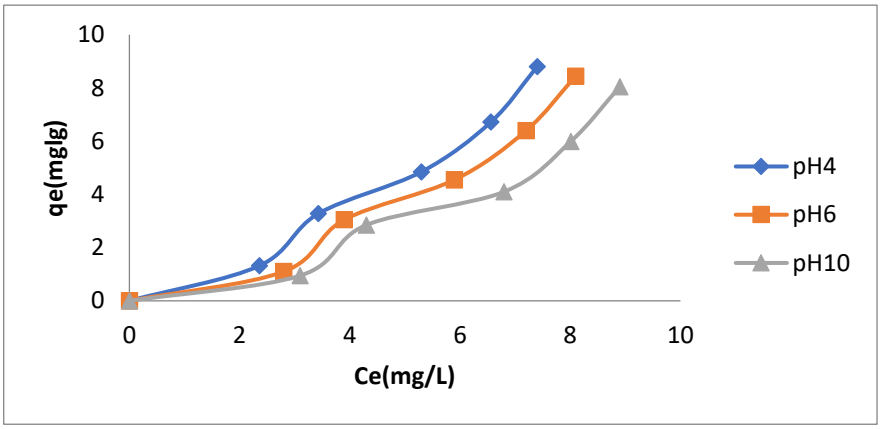

Figure 6. Effect of pH on removal of DY

As can be shown, the largest amount of dye removed occurred at pH 4. The results collected can be clarified by the fact that the molecular structure of DY in solution medium varies significantly across the pH spectrum (4-10). Since the maximal adsorption occurred at pH 4, all DY8 adsorption tests were conducted at this pH (Ferreira MM et al, 2016).

Adsorption Isotherms

The most critical piece of knowledge is the adsorption isotherm, which shows how molecules are dispersed between the liquid and solid phases as adsorption achieves equilibrium. Adsorption was carried out at initial concentrations ranging from 5 to 25 ppm at a temperature of 298 K. The outcome is visualized in **Figure 7**.

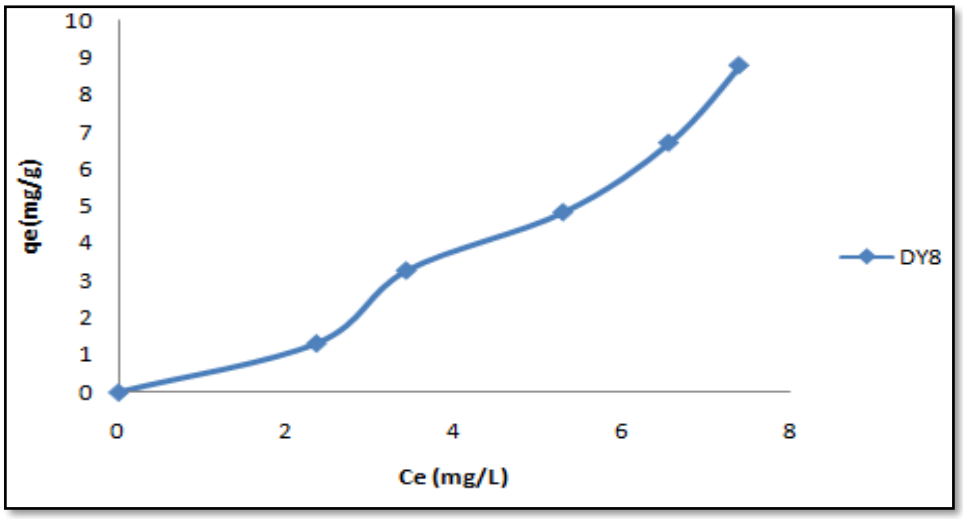

Figure 7. Adsorption isotherms of DY8 on clay at, (25) °C.

As shown, both of these adsorption isotherms were of the S type, meaning that the adsorbent is either mesoporous or nonporous and has strong adsorption energy. Additionally, this indicates that the adsorbate is vertical or flat in orientation and that the adsorbent is nonfunctional. (Casandra A et al, 2015). Adsorption data provide insight into the adsorbent's effectiveness, adsorption isotherms, and the equilibrium distribution of a solute between adsorbent and solution, allowing for the estimation of adsorbent efficiency and expense. This thesis examined three of the most often-used isotherm equations, namely the Langmuir and Freundlich equations. The experimental results obtained were also compared to the Freundlich equation's linear form [(equation 2]. The linear plots of log qe versus log Ce in

Figure 8 illustrate the Freundlich isotherm in action. The values of 1n and Kf are determined by the slope and intercept of the plots, as seen in (Table 8) (Muhammad J et al, 2007; El said S et al, 2014).

$$\ln q_e = \ln K_f + \mathbf{1/n} \ln C_e \qquad (2)$$

Where qe denotes the equilibrium concentration of dye in the solid phase (mg g-1), Ce denotes the equilibrium concentration of dye in solution (mg L-1), 1n is constants denote the parameters affecting the adsorption power, and Kf denotes the adsorption rate.

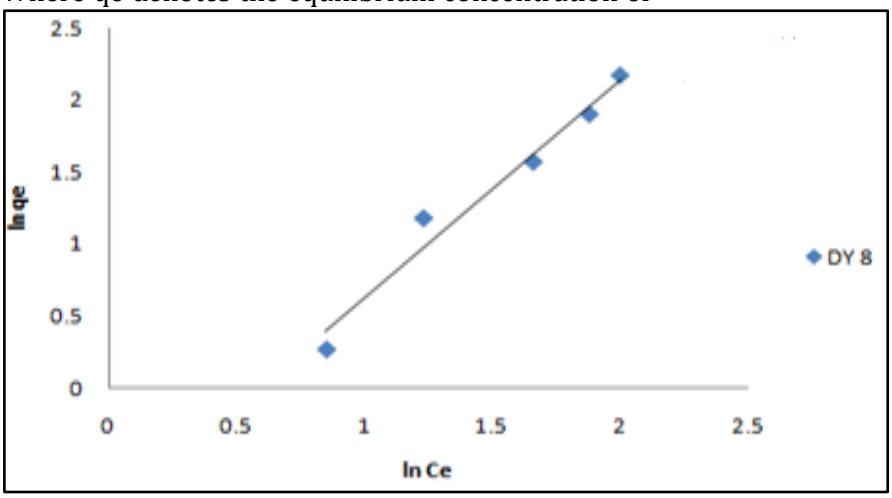

Figure 8. The Freundlich model of a linear plot

The Langmuir model has been successfully extended to a variety of real-world sorption systems. It is represented mathematically as [Eq. 3 (El-Mahdy M. M et al, 2007; Gueu S et al, 2007).

$$\mathbf{C_e/q_e = 1/q_m k_L + C_e/q_m} \qquad (3)$$

The Langmuir constants q m and kL are related to the performance of adsorption and the capacity of adsorption, respectively (Erdem, B et al, 2016). The linear plots of Ce/qe versus Ce demonstrate the application of the Langmuir isotherms (**Figure 9**). Additionally, the slope and intercepts were used to determine the values of qm and kL. The parameters obtained from the two isotherms for DY8 adsorption clay are mentioned in Table (1).

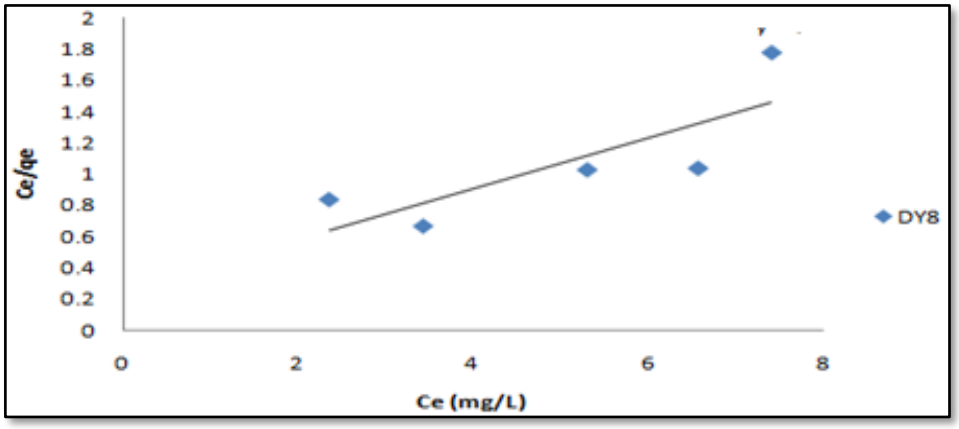

Figure 9. The linear plot of Langmuir isotherm

Table 1. The parameters obtained of the four isotherms for DY8 adsorption clay.

angmuir	**q_m (mg/g)**	**K_L (mg/l)$^{-1}$**	**R_L**	**R^2**
	6.17	**0.632**	**0.059**	**0.650**
Freundlich	**n**	**K_f (L. g^{-1})**		**R^2**
	0.65	**0.40**		**0.969**

When R2 values from Langmuir and Freundlich plots are compared, it is clear that the experimental data suits the Freundlich isotherms the better. (RL) was also calculated using the equation RL =1 / (1+KLC0). The RL value obtained is 0.059, indicating that 0 RL > 1, indicating that adsorption happens normally at 298 K. Additionally, the strong Kf value (0.40) showed that the adsorbent had a

high potential for the adsorption of DY (Lee C et al, 1984). The Freundlich constant value of n= 0.65, n (1< n <10) indicates that clay has a strong affinity for DY8 molecules.

Thermodynamic Calculations

To get a deeper understanding of how temperature affects adsorption, it is necessary to research the thermodynamic parameters of adsorption, including ΔHo, ΔSo and ΔGo. ΔHo has been determined for all adsorption processes using the Van's Hoff equation (equation (4) (Piccin J et al, 2011) by plotting the logarithmic value of the adsorption equilibrium constant (Keq) against the temperature as (1/T).

$$\ln K_{eq} = \frac{-\Delta H^{\circ}}{RT} + \frac{\Delta S^{\circ}}{R} \qquad (4)$$

The gas constant is represented by R. ln Keq should have a linear relationship with 1/T (in Kelvin). The Van's Hoff plot has a slope equivalent to -ΔH/R and an intercept equal to ΔS/R. The obtained values for ΔHo and ΔS are shown in Table (2), along with the Gibbs free energy of adsorption (ΔGo), which is determined using the following equation (5) (Nichola C et al, 2012; Gueu S et al, 2007) **Figure 10**.

$$\Delta G^{\circ} = -\Delta H^{\circ} - T\Delta S \qquad (5)$$

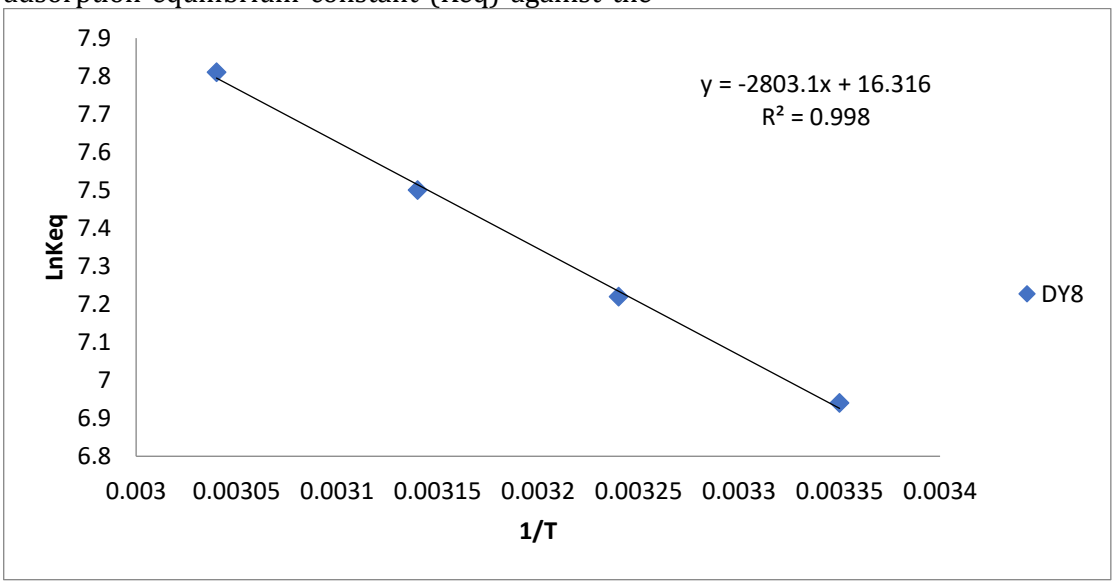

Figure 10. Vant Hoff plot of the dye onto the clay

Table 2. Thermodynamic parameters of the DY adsorption on clay at 20(mg/ L).

ΔH°kJ/mol	ΔS°J/Kmol	ΔG° kJ/mol			
		298 K	308 K	318 K	328 K
-0.33	19.55	-6.16	6.35-	-6.55	-6.74

The data in Table (4) suggest that the values of the difference in (ΔG) for dye adsorption on clay are negative at all measured temperatures (298-328) K, indicating that dye adsorption on clay occurred spontaneously and in a thermodynamically favorable manner. ΔG decreased (increasingly negative) as the temperature rose from (2983-328) K, implying that spontaneously increased as temperature increased. The fact that the three systems have negative ΔH values indicates that the dye adsorption onto clay was an exothermic operation. Additionally, the positive ΔS indicates that the degrees of freedom at the solid-liquid interface improved during dye adsorption onto the clay. To a certain degree, physisorption and chemisorption may be categorized according to the magnitude of the enthalpy transition. Usually, values of ΔH 40 kJ / moles are regarded as physisorption [Karaca, S et al, 2004; Blanchard, G et al, 1984].

Adsorption Kinetic

The adsorption kinetics of 20 mg/L dye onto clay at 298K was investigated using three commonly used kinetic models: the Laguerre pseudo-first-order equation (equation r), the pseudo-second-order equation (equation 6), and the intraparticle diffusion equation [Tran H. N et al, 2017; El-Mahdy et al, 2020]. (Equation 7) and the resulting data are summarized in Table 4 and depicted in Figure 10.

$$\ln(q_e - q_t) = \ln q_e - k_1 t \qquad (5)$$

$$\frac{t}{q_t} = \frac{1}{k_2 q_e^2} + \frac{1}{q_e} t \qquad (6)$$

$$q_t = K_D t^{1/2} + c \qquad (7)$$

Where qe is the equilibrium adsorption potential

(mg g-1), qt is the time-dependent adsorption capacity, k1 is the pseudo-first-order model's rate constant (min-1), and K2 is the pseudo-second-order model's rate constant (mg min-1). The initial adsorption rate is described as h= k2 qe2. kD denotes the intraparticle diffusion rate constant (mg g-1 min-1/2), and C denotes the intercept. The constants qe, k1, k2, and kD are determined using the slopes and intercepts of the three equations' linear plots (**Figure 11**) in addition to the h value listed in Table 3.

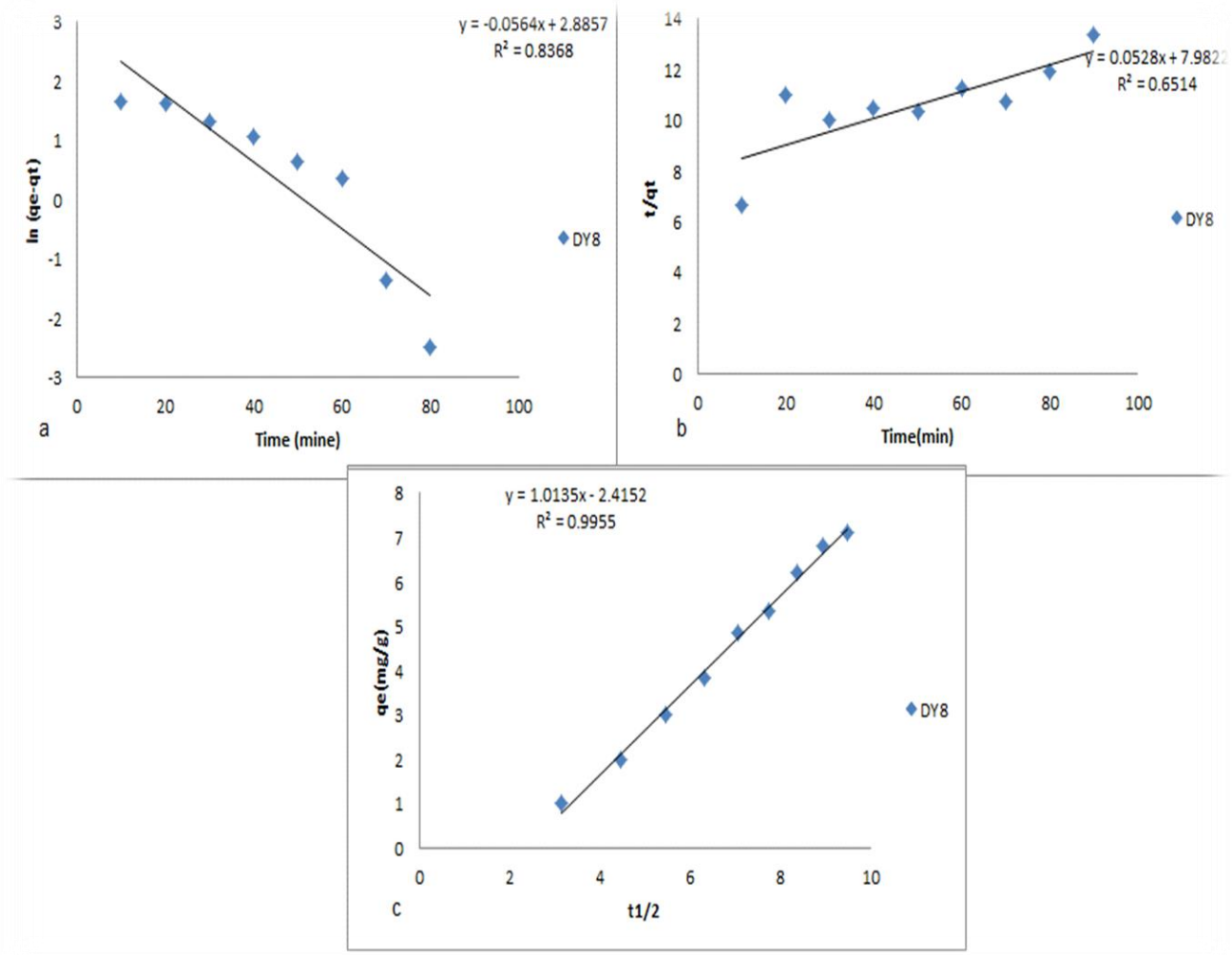

Figure 11. The liner plot of a) pseudo-first, b) second-order kinetics c) intraparticle diffusion models of DY8 adsorption at 20 (ppm).

The correlation coefficient (R2) values in Table 4 indicate that the adsorption process follows a pseudo-first-order model. Additionally, the plot of the intra-particle diffusion model demonstrates that the straight line extrapolated to the origin did not enter the origin, indicating that the intraparticle diffusion stage is not the only rate-controlling step but that many other stages play a significant role.

Table 3. Comparison of the pseudo-first, second-order kinetics, and intraparticle diffusion models of DY8 adsorption at 20 (ppm).

T (ºC)	q_e (exp.)	pseudo-first -order			pseudo-second –order				intrapartical diffusion	
		q_e(calc.)	K_1	R^2	q_e(calc.)	K_2	h	R^2	K_D	R^2
298	6.75	17.9	0.056	0.836	18.93	0.00349	0.125	0.651	1.013	0.995
T (ºC)	q_e (exp.)	pseudo-first -order			pseudo-second –order				intrapartical diffusion	
		q_e(calc.)	K_1	R^2	q_e(calc.)	K_2	h	R^2	K_D	R^2
298	6.75	17.9	0.056	0.836	18.93	0.00349	0.125	0.651	1.013	0.995

Quantum Studies

The structure of the DY8 dye and the active adsorption site were optimized using theoretical calculations. In **Figure 11**, the HOMO (High Occupied Molecular Orbital) (donate electron orbital) and LUMO (Low Occupied Molecular Orbital) (accept electron orbital) orbitals, as well as the HOMO-LUMO orbitals and the optimized structure of DY8 dye, were seen. The energy gap (ΔE= ELUMO-EHOMO) between the boundary orbits is another critical element in describing molecular behavior; therefore, when the energy gap is reduced, the activity is improved (Mustafa M. Kadhim et al, 2020). The energy difference has a value of (0.20321). The electron density was referred to as the overall electron density (TED); red-colored locations indicated a negative charge, which corresponds to the electronegativity of the N, S, and O atoms inside the DY8 dye molecule; this is an electrophilic attack, while the blue zone shows the strongest positive area capable of accepting electrons from the donor compound (**Figure 12**).

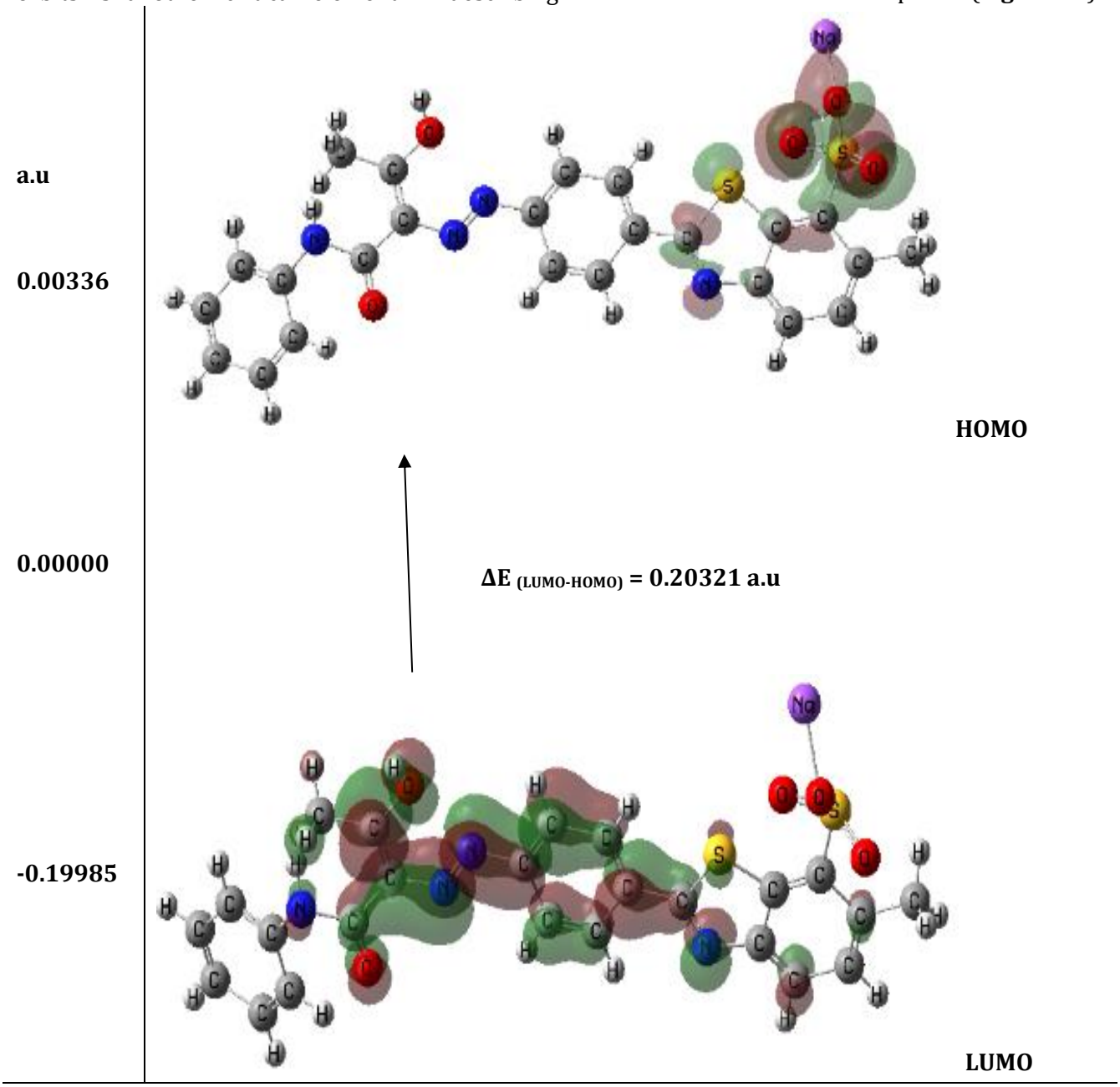

Figure 12. HOMO-LUMO molecule orbitals energies of DY8

The electrostatic surface potential (ESP) indicates the position of the molecule's adsorption on the metal surface, which matches with the direction of the carbonyl group, oxygen, nitrogen, and sulfur atoms. Figure 13 shows the ESP of the DY8.

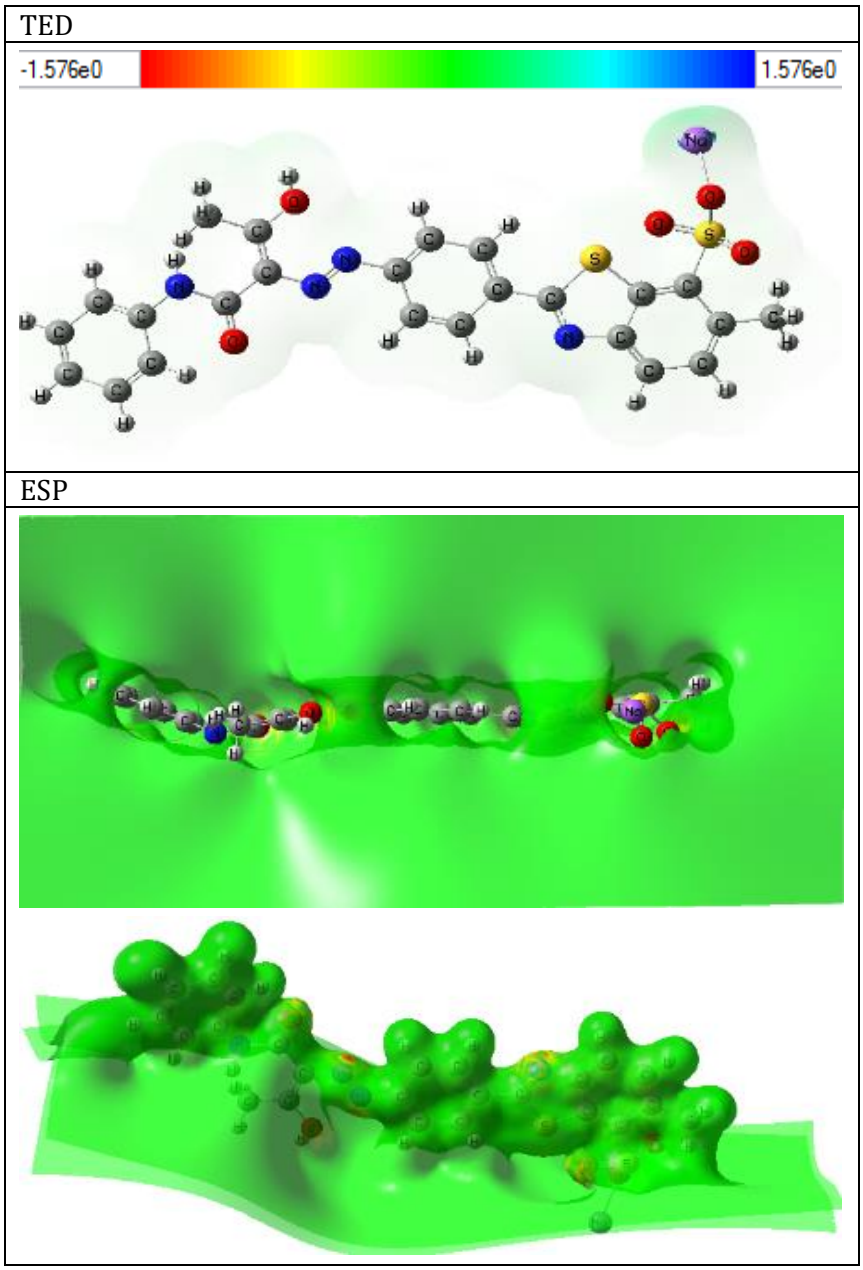

Figure 13. TED and ESP maps of DY8 structuree

Conclusions

The primary assumptions that can be taken from the previous observations and explanation are as follows: adsorption systems can be described by electrostatic attraction (physical adsorption). The results of the kinetics examination indicate that dye adsorption on clay ideally suits the pseudo-first-order model, while DY8 dye was better suited to the Freundlich isotherm for equilibrium adsorption. Additionally, the thermodynamic analysis indicates that all of the systems studied were random and exothermic, based on the values of ΔG and ΔH. While DFT calculations suggested that RS dye molecules possess an optimal location for adsorption onto clay through the interaction of their electrons with the clay, these observations were corroborated by experimental evidence.

References

Adeyemo AA, Adeoye IO, Bello OS. Adsorption of dyes using different types of clay: a review. *Applied Water Science*, 2017; 7(2): 543-568. https://doi.org/10.1007/s13201-015-0322-y

Becke AD. Density-functional thermochemistry. III. The role of exact Exchange. *Chemical Physics* 1993; 98: 5648.

Blanchard G, Maunaye M, Martin G. Removal of heavy metals from waters by means of natural zeolites. *Water research* 1984; 18(12): 1501-1507.

Casandra A, Noskov BA, Hu MY, Lin SY. Adsorption kinetics of heptadecafluoro-1-nonanol: Phase transition and mixed control. *Journal of colloid and interface science* 2018; 527, 49-56.

Chandrasekhar, S, Pramada, P. N. (2006). Rice husk ash as an adsorbent for methylene blue—effect of ashing temperature. *Adsorption* 12(1): 27-43.

Colpini LMS, Alves HJ, Dos Santos OAA, Costa CMM. Discoloration and degradation of textile dye aqueous solutions with titanium oxide catalysts obtained by the sol–gel method. *Dyes and Pigments* 2008; 76(2): 525-529.

Derudi M, Venturini G, Lombardi G, Nano G, Rota R. Biodegradation combined with ozone for the remediation of contaminated soils. *European Journal of Soil Biology* 2007; 43(5-6): 297-303.

Doadrio AL, Salinas A, Sánchez-Montero JM, Vallet-Regi M. Drug release from ordered mesoporous silicas. *Current pharmaceutical design*, 2015; 21(42): 6213-6819.

Dos Santos OAA, Castellib CZ, Oliveirab MF, de Almeida Netob AF, Da Silvab MG. Adsorption of synthetic orange dye wastewater in organoclay. *Chemical Engineering* 2013; 32: 307-312.

El-Mahdy MM, Raslan HY, Hassan AM. Physicochemical Studies on Interacting Some Cardiovascular Drug Pairs. *Journal of advanced Biomedical and Pharmaceutical Sciences* 2020; 3(3): 135-149.

El-Shafey ESI, Al-Lawati HA, Al-Hussaini AY. Adsorption of fexofenadine and diphenhydramine on dehydrated and activated carbons from date palm leaflets. *Chemistry and Ecology* 2014; 30(8): 765-783.

Erdem B, Erdem M, Özcan AS. Adsorption of Reactive Black 5 onto quaternized 2-dimethylaminoethyl methacrylate based polymer/clay nanocomposites. *Adsorption* 2016; 22(4-6): 767-776.

Ferreira MM. *Multivariate Encyclopedia of Physical Organic Chemistry* 2016; (2): 1-38.

Garbett NC, Chaires JB. Thermodynamic studies for drug design and screening. *Expert opinion on drug discovery* 2012; 7(4): 299-314.

Gece G. The use of quantum chemical methods in corrosion inhibitor studies. *Corrosion Science* 2008; 50(11): 2981-2992.

Gueu S, Yao B, Adouby K, Ado G. Kinetics and thermodynamics study of lead adsorption on to activated carbons from coconut and seed hull of the palm tree. *International Journal of Environmental Science & Technology* 2007; 4(1): 11-17.

Hussein EA, Shaheed IM, Hatam RS, Kadhim MM, Al-Kadhum DT, Abd AL-kareem E. Adsorption, Thermodynamic and DFT Studies of Removal RS Dye on the Iraq Clay from Aqueous Solutions. *Systematic Reviews in Pharmacy* 2020; 11(3): 495-502.

Iqbal MJ, Ashiq MN. Adsorption of dyes from aqueous solutions on activated charcoal. *Journal of Hazardous Materials* 2007; 139(1): 57-66.

Kadhim MM, Kubba RM. Theoretical Investigation on Reaction Pathway, Biological Activity, Toxicity and NLO Properties of Diclofenac Drug and Its Ionic Carriers. *Iraqi Journal of Science* 2020; 61(5): 936-951.

Karaca S, Gürses A, Açıkyıldız M, Ejder M. Adsorption of cationic dye from aqueous solutions by activated carbon. *Microporous and Mesoporous materials* 2008; 115(3): 376-382.

Kareem SH, Al-Hussien EABD. Adsorption of Congo, Red Rhodamine B and Disperse blue dyes from aqueous solution onto raw flint clay. *Baghdad Science Journal* 2012; 9(4): 680-688.

Kareem SH. Magnetic mesoporous silica material (Fe3O4@ mSiO2) as adsorbent and delivery system for ciprofloxacin drug. In *IOP Conference Series: Materials Science and Engineering* 2020; 871(1): 012020.

Kareem A, Alrazak NA, Aljebori KH, Aljeboree AM, Algboory HL, Alkaim AF. Removal of methylene blue dye from aqueous solutions by using activated carbon/ureaformaldehyde composite resin as an adsorbent. *International Journal of Chemical Sciences* 2016; 14(2): 635-648.

Kausar A, Iqbal M, Javed A, Aftab K, Bhatti HN, Nouren S. Dyes adsorption using clay and modified clay: a review. *Journal of Molecular Liquids* 2018; 256, 395-407.

Lee C, Yang W, Parr RG. Development of the Colle-Salvetti correlation-energy formula into a functional of the electron density. *Physical review B* 1988; 37(2): 785.

McIver Jr, JW, Komornicki A. Structure of transition states in organic reactions. General theory and an application to the cyclobutene-butadiene isomerization using a semiempirical molecular orbital method. *Journal of the American Chemical Society* 1972; 94(8): 2625-2633.

Piccin JS, Dotto GL, Pinto LAA. Adsorption isotherms and thermochemical data of FD&C Red n 40 binding by chitosan. *Brazilian Journal of Chemical Engineering*, 2011; 28(2): 295-304.

Tran HN, You SJ, Hosseini-Bandegharaei A, Chao HP. Mistakes and inconsistencies regarding adsorption of contaminants from aqueous solutions: a critical review. *Water research* 2017; 120, 88-116.

Udhayakala P, Jayanthi A, Rajendiran TV. Adsorption and quantum chemical studies on the inhibition potentials of some formazan derivatives. *Der Pharma Chemica* 2011; 3(6): 528-539.

Von Barth, U. (2004). Basic density-functional theory—an overview. *Physica Scripta* 2004; (T109): 9.

Weigend F, Ahlrichs R. Balanced basis sets of split valence, triple zeta valence and quadruple zeta valence quality for H to Rn: Design and assessment of accuracy. *Physical Chemistry Chemical Physics* 2005; 7(18): 3297-3305.

Yuh-Shan H. Citation review of Lagergren kinetic rate equation on adsorption reactions. *Scientometrics* 2004; 59(1): 171-177.

Zhang F, Zhao J, Shen T, Hidaka H, Pelizzetti E, Serpone N. TiO2-assisted photodegradation of dye pollutants II. Adsorption and degradation kinetics of eosin in TiO2 dispersions under visible light irradiation. *Applied Catalysis B: Environmental* 1998; 15*(*1-2): 147-156.

Majumdar S, Roy S. Relevance of quantum mechanics in bacterial communication. *NeuroQuantology* 2018; 16(3): 1-6.